Proceedings of IMECE04
2004 ASME International Mechanical Engineering Congress and Exposition
November 13-20, 2004, Anaheim, California USA

IMECE2004-59492

STIFFNESS EVALUATION AND VIBRATION IN A TRACTOR GEAR

G. BONORI
Dipartimento di Ingegneria Meccanica e Civile,
Università di Modena e Reggio Emilia, I-41100
Modena, Italy
bonori.giorgio@unimore.it

A.O. ANDRISANO
Dipartimento di Ingegneria Meccanica e Civile,
Università di Modena e Reggio Emilia, I-41100
Modena, Italy
andrisano.angelo@unimore.it

F. PELLICANO
Dipartimento di Ingegneria
Meccanica e Civile, Università di
Modena e Reggio Emilia, I-41100
Modena, Italy
francesco.pellicano@unimore.it

ABSTRACT

The problem of gear noise in vehicles has been intensively studied in the past; however, recently the interest about this problem grew because of great restrictions in the laws regarding noise level and the increase of international competition. One of the most important vibration and noise sources is transmission error that excites the gearbox as a dynamic system, the gearbox surfaces, and connected components; the external box radiates noise. However, the current understanding of gear vibration remains incomplete, even though there is general agreement about the nature of the phenomenon. Vibrations are due to several sources: torsion resonance, impulsive or cyclic fluctuations in drive torque, gear mesh transmission error, local component vibration responses and fluctuations in the output torque demand.

The concept of a vibrating system made of two gears is generally modeled through two wheels linked by the teeth mesh stiffness. In its simplest form, this model can simulate the classical linear resonance, i.e. the resonant frequency of the system. However, more complex phenomena such as parametric instabilities can be an important source of noise.

In the present paper vibration problems in the gears of an industrial vehicle are investigated through the use of perturbation technique. A suitable software has been developed to generate the gear profiles in order to evaluate global mesh stiffness using finite element analysis.

INTRODUCTION

In the analysis of gear dynamics several engineering topics are generally considered: geometric profile/surface generation, kinematics; gear tooth, shaft and support elasticity; linear and nonlinear dynamical interactions.

In the past several approaches have been proposed for gear modeling. An interesting literature overview can be found in [1], where the mathematical models used in gear dynamics were classified by considering: the evaluation of simple dynamic factor; tooth compliance; gear dynamics; geared motor dynamics; and torsion vibration.

Helical gears were studied by Andersson and Vedmar [2], teeth impact problems were investigated by Yan and Sun [3], the flexibility of shafts using a multi-degrees of freedom model was analyzed by Lin et al. [4,5]. Cai and Hayashi [6] proposed a linear approximation for a pair of spur gears and compared the analytical solution with the numerically calculated result by the nonlinear equation; they found that linear models are able to capture the main dynamic phenomena. Parker et al. [7] studied the nonlinear dynamic response of a spur gear pair using a semi-analytical approach and two single degrees of freedom models. Amabili and Rivola [8] obtained a continuous closed form solution for any rotational speed and computed the transition curves, stable and unstable regions, by means of the Hill infinite determinant.

The evaluation of the model parameters as mesh stiffness, mesh damping and transmission error is another important aspect of gear modeling: finite element analysis, analytical models and experiments are the commonly used approaches. Ming-Haung Tsai and Ying-Chien Tsai [9] compared FEM result with the Houser and Tavakoli's [10] analytical technique for a plastic spur gear pair. Howards et al. [11] used FEM to ascertain the dynamical effect of different types of gear train damage.

One of the main problems in using FEM is the geometry generation; in particular, a good tooth profile and tooth root fillet generation is quite important to obtain reliable results. Such generation can be obtained from analytical or numerical approaches. Existence conditions for envelope curves were intensively studied by Zalgaller and Litvin [12]. Litvin et al. [13] focused their attention on gear profiles, and proposed methods for finding spurious envelope solutions.

In the present paper, software has been developed to build the teeth profile. The software is able to generate a very large classes of 2D gears, starting from any rack shape. Using this technique the tooth fillet profile, including undercutting, can be modeled. Then a single degree of freedom system has been developed for the dynamic modeling. The stiffness of the gears is calculated using commercial finite element software (FEM) for different meshing positions of a gear pair, using contact elements for the teeth interaction. This approach allows one to accurately evaluate the variable global stiffness, which depends on the gear position, materials and teeth geometry. The variable stiffness gives rise to a parametric excitation, which is periodic; therefore it gives rise to a Mathieu type instability. A Fourier series of the variable stiffness is obtained from the numerical data evaluated with the FEM model. The dynamic model is analyzed by means of perturbation techniques [14].

MESHING EQUATIONS

Let us consider the profile generation by means of an envelope of a rack profile σ_1, see fig. 1. Three references systems are introduced:

- S_f ($O_f x_f y_x$) fixed reference;
- S_1 ($O_1 x_1 y_1$) moving respect to S_f;
- S_2 ($O_2 x_2 y_2$) moving respect to S_f;

where σ_1 is fixed in S_1 and σ_2 is fixed in S_2.
θ is local variable that identify a point on the curve σ_1 and $\underline{\phi}$ is local variable that identify a point on the curve σ_2. The parameter $\underline{\phi}$ depends on ϕ; P_1 and P_2 are the same point P represented in the reference systems S_1 and S_2.

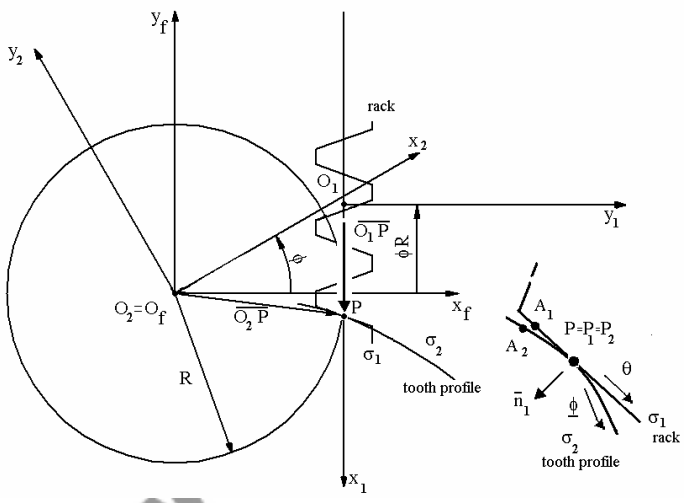

Fig. 1: Reference systems

Let us consider a regular plane curve σ_1 describing the rack tooth profile. The tooth profile (σ_2) is described by the meshing equation:

$$f(\theta,\phi)=\bar{n}_1(\theta)\cdot\bar{v}_\tau(\theta,\phi)=0 \tag{1}$$

this equation states that the sliding velocity $\bar{v}_\tau$, of S_2 with respect to S_1, has to be normal to the enveloping curve σ_1.

Moreover one can express the normal vector to curve σ_1 as:

$$\bar{n}_1(\theta)=\bar{k}_1\times\frac{\partial}{\partial\theta}\overline{O_1P_1}(\theta) \tag{2}$$

Using homogeneous coordinates, P_1 on σ_1 is described by vector $\overline{O_1P_1}$. The following regularity conditions of the curve are imposed:

$$\overline{O_1P_1}(\theta)\in C^1,\quad \frac{\partial\overline{O_1P_1}}{\partial\theta}(\theta)\neq\bar{0} \tag{3}$$

Assuming that S_1 is fixed and S_2 is moving with respect to S_1, the sliding velocity of P in S_1 becomes:

$$\bar{v}_\tau(P_1)=\frac{d}{dt}\overline{O_1O_2}+\bar{\omega}\times\overline{O_2P_1}=\frac{d}{dt}\overline{O_1O_2}+\bar{\omega}\times\left(\overline{O_2O_1}+\overline{O_1P_1}\right) \tag{4}$$

In order to describe the vector $\overline{O_1P_1}(\theta)$ in the reference S_2 a transformation matrix M_{21} must be considered:

$$\overline{O_2P_2}(\theta,\phi)=M_{21}(\phi)\cdot\overline{O_1P_1}(\theta) \tag{5}$$

$\mathbf{M}_{21}$ transforms reference system 1 to 2 by expressing the motion of S_1 and S_2 with respect to S_f using the Lagrange

parameter ϕ. Equation (5) represents a family of curves, which describe the trajectories of the points of σ_1 while θ is varying during the motion respect to S_2. Equation (1) allows to reduce the family of curves to a unique curve σ_2, which is the envelope of σ_1. Equation (1) and (5) are sufficient to determinate the tooth profile curve σ_2 as function of ϕ.
According to Litvin, et al. [13], the following sufficient conditions for the existence and regularity of the curve must be respected:
1) The family of curves σ_2 must have C^2 regularity for both θ and ϕ parameters:

$$\overline{O_2P_2}(\theta,\phi)\in C^2, \quad \theta\in E\subseteq R, \quad \phi\in(a,b) \tag{6}$$

2) σ_1 must be regular:

$$\frac{\partial}{\partial\theta}\overline{O_1P_1}(\theta_0)\neq\bar{0} \tag{7}$$

3) If a generic point (θ_0,ϕ_0) verifies eq. (1), then it cannot be a singular point and must verify the following equation:

$$\frac{\partial}{\partial\theta}\overline{O_1P_1}(\theta)\frac{\partial}{\partial t}\theta(t_0)+\bar{v}_\tau(\theta_0,\phi_0)\neq\bar{0} \tag{8}$$

where $\theta=\theta(t)$ provides the contact point on σ_1 while θ is varying.

APPLICATION OF THE ANALYTICAL ENVELOPING METHOD

Sliding velocity
From fig. 1 one obtains that:

$$\overline{O_1O_2}=R\phi\bar{i}_1-R\bar{j}_1=\begin{bmatrix}R\phi & -R & 0 & 0\end{bmatrix}^T \tag{9}$$

and

$$\bar{\omega}=\begin{bmatrix}0 & 0 & \omega & 0\end{bmatrix}^T, \quad \omega=\frac{d}{dt}\phi(t) \tag{10}$$

the sliding velocity given by eq. (4) becomes:

$$\bar{v}_\tau(P)=R\,\omega\bar{i}_1+\begin{vmatrix}\bar{i}_1 & \bar{j}_1 & \bar{k}_1\\ 0 & 0 & \omega\\ -R\phi & +R & 0\end{vmatrix}+\begin{vmatrix}\bar{i}_1 & \bar{j}_1 & \bar{k}_1\\ 0 & 0 & \omega\\ (O_1P)_{x1} & (O_1P)_{y1} & 0\end{vmatrix} \tag{11}$$

Roto-translation matrix
The rotation matrix is given by:

$$R_z(\eta)=\begin{bmatrix}\cos(\eta) & -\sin(\eta) & 0 & 0\\ \sin(\eta) & \cos(\eta) & 0 & 0\\ 0 & 0 & 1 & 0\\ 0 & 0 & 0 & 1\end{bmatrix} \tag{12}$$

where η is a generic rotation angle.
The translation of point P can be described by the translation matrix:

$$P+\bar{t}=\begin{bmatrix}P_x+t_x\\ P_y+t_y\\ P_z+t_z\\ 1\end{bmatrix}=\begin{bmatrix}1 & 0 & 0 & t_x\\ 0 & 1 & 0 & t_y\\ 0 & 0 & 1 & t_z\\ 0 & 0 & 0 & 1\end{bmatrix}\begin{bmatrix}P_x\\ P_y\\ P_z\\ 1\end{bmatrix}=T_t\,P \tag{13}$$

where $\bar{t}$ is a vector indicating the translation.
Finally, defining η=-ϕ−π/2 and $\bar{t}=\overline{O_1O_2}$ the complete roto-traslation matrix becomes:

$$M_{21}(\phi)=\begin{bmatrix}-\sin(\phi) & \cos(\phi) & 0 & R(\phi\sin(\phi)+\cos(\phi))\\ -\cos(\phi) & -\sin(\phi) & 0 & R(\phi\cos(\phi)-\sin(\phi))\\ 0 & 0 & 1 & 0\\ 0 & 0 & 0 & 1\end{bmatrix} \tag{14}$$

Rack protuberance parameters
Figure 2 shows the rack and protuberance parameters according to UNI 8862/2 [15]:

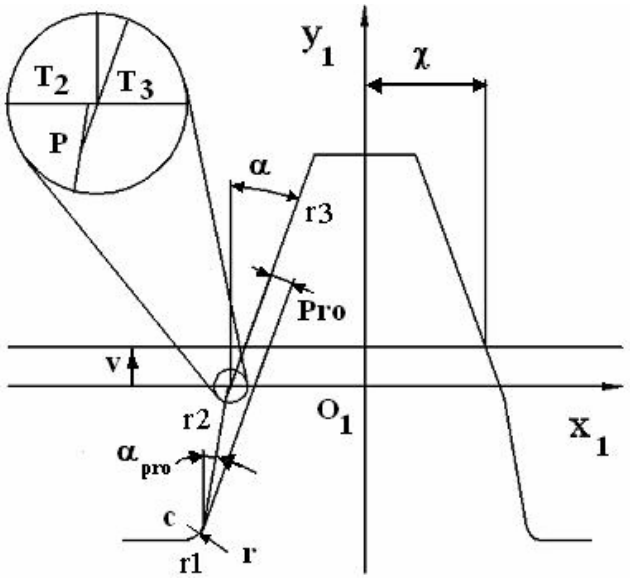

Fig. 2: Rack protuberance parameters

Both tooth profiles are constituted by three regular curves: a circular arc (r1) and two rectilinear segments (r2) and (r3). Such profile is defined by means of the following parametric equations, written in terms of the parameters θ_1, θ_2 and θ_3

$$(r1)\ \begin{cases} x_1 = x_C + r\ \cos\left(\dfrac{\theta_1}{r}\right) \\ y_1 = y_C + r\ \sin\left(\dfrac{\theta_1}{r}\right) \end{cases} \tag{15}$$

$$(r2)\ \begin{cases} x_1 = x_{T2} + \theta_2\ \sin(\alpha_{Pro}) \\ y_1 = \theta_2\ \cos(\alpha_{Pro}) \end{cases} \tag{16}$$

$$(r3)\ \begin{cases} x_1 = x_{T3} + \theta_3\ \sin(\alpha_n) \\ y_1 = \theta_3\ \cos(\alpha_n) \end{cases} \tag{17}$$

where:

$$\begin{aligned} \chi &= \frac{\pi m}{4} \\ x_C &= -\chi + \frac{P_{ro}}{\cos(\alpha_n)} - (h\,m - r + r\sin(\alpha_n))tg(\alpha_n) - r\cos(\alpha_n) \\ y_C &= -h\,m + v + r \\ x_{T2} &= x_C + r\cos(\alpha_{Pro}) + (h\,m - v - r + r\sin(\alpha_{Pro}))tg(\alpha_{Pro}) \\ x_{T3} &= -\chi - v\,tg(\alpha_n) \end{aligned} \tag{18}$$

are the coordinates of the C, T_2 and T_3 points indicated in fig. 2. The three curves, which constitute the whole rack profile, are defined in the following intervals:

$$(1)\ \theta_1 \in \left[\theta_{11} = -\frac{\pi}{2}r; \theta_{12} = -\alpha_{pro}r\right]$$

$$(2)\begin{cases} \theta_2 \in \left[\theta_{21} = \dfrac{-(hm - v - r + r\sin(\alpha_{pro}))}{\cos(\alpha_{pro})}; \theta_{22} = \dfrac{x_{T3} - x_{T2}}{\sin(\alpha_{pro}) - \cos(\alpha_{pro})tg(\alpha_n)}\right] if\ \alpha_{pro} \neq \alpha_n \\ \theta_2 \in \left[\theta_{21} = \dfrac{-(hm - v - r + r\sin(\alpha_n))}{\cos(\alpha_n)}; \theta_{22} = \dfrac{-(hm - v - r + r\sin(\alpha_n))}{\cos(\alpha_n)}\right] if\ \alpha_{pro} = \alpha_n \end{cases}$$

$$(3)\begin{cases} \theta_3 \in \left[\theta_{31} = \dfrac{1}{\cos(\alpha_n)}\dfrac{x_{T3} - x_{T2}}{tg(\alpha_{pro}) - tg(\alpha_n)}; \theta_{32} = \dfrac{hm + v}{\cos(\alpha_n)}\right] if\ \alpha_{pro} \neq \alpha_n \\ \theta_3 \in \left[\theta_{31} = \dfrac{-(hm - v - r + r\sin(\alpha_n))}{\cos(\alpha_n)}; \theta_{32} = \dfrac{hm + v}{\cos(\alpha_n)}\right] if\ \alpha_{pro} = \alpha_n \end{cases} \tag{19}$$

Involute profile generated from a rectilinear segment
Using eq. (16) or eq. (17) yields

$$\overline{O_1P_1} = \begin{bmatrix} x_T + \theta\sin(\alpha) \\ \theta\cos(\alpha) \\ 0 \\ 1 \end{bmatrix} \tag{20}$$

which can be inserted in (1). Therefore the equation of mesh becomes:

$$\omega[\theta + (x_T - R\phi)\sin(\alpha)] = 0 \tag{21}$$

which gives

$$\theta(\phi) = (R\phi - x_T)\sin(\alpha) \tag{22}$$

Substituting (22) into (5) one obtains

$$\begin{cases} x\ (\phi) = R\cos(\phi) + (R\phi - x_T)\cos(\alpha)\sin(\alpha + \phi) \\ y\ (\phi) = -R\sin(\phi) + (R\phi - x_T)\cos(\alpha)\cos(\alpha + \phi) \end{cases} \tag{23}$$

Profile generated from rack tooth fillet
Equation (15) yields

$$\overline{O_1P_1} = \begin{bmatrix} x_C + r\cos\left(\dfrac{\theta_1}{r}\right) \\ y_C + r\sin\left(\dfrac{\theta_1}{r}\right) \\ 0 \\ 1 \end{bmatrix} \tag{24}$$

which can be inserted in (1). Therefore, the equation of mesh (1) becomes

$$\omega\left[y_C\cos\left(\frac{\theta}{r}\right) + (R\phi - x_C)\sin\left(\frac{\theta}{r}\right)\right] = 0 \tag{25}$$

Solving eq. (25) with respect to θ, four solutions can be found in the interval $[-\pi, \pi]$:

$$\theta_{1,2,3,4} = \pm\arccos\left[\pm\frac{|x_C - R\phi|}{\sqrt{y_C^2 + (x_C - R\phi)^2}}\right] \tag{26}$$

according to eq.s (19) only the following solution is acceptable:

$$\theta = -\arccos\left[\frac{|x_C - R\phi|}{\sqrt{y_C^2 + (x_C - R\phi)^2}}\right] \tag{27}$$

Substituting (27) into (5) yields

$$\begin{cases} x\ (\phi) = A\cos(\phi) + B\sin(\phi) \\ y\ (\phi) = B\cos(\phi) + A\sin(\phi) \end{cases} \tag{28}$$

$$A = R + y_C - r\sqrt{\frac{y_C^2}{y_C^2 + (x_C - R\phi)^2}}$$
$$B = R\phi - x_C - \frac{r\sqrt{(x_C - R\phi)^2}}{\sqrt{y_C^2 + (x_C - R\phi)^2}} \qquad (29)$$

Equations (23) and (28) represent the curves that generate the tooth profile from the rack cutter envelope.

Limitsϕ values

The three curves r1, r2 and r3 generate three profiles t1, t2 and t3, see fig. 3. The boundaries of the curves r1, r2 and r3, in terms of their parameters θ_1, θ_2 and θ_3 are reflected on the boundaries of the envelopes t1, t2 and t3, in terms of ϕ_1, ϕ_2 and ϕ_3.

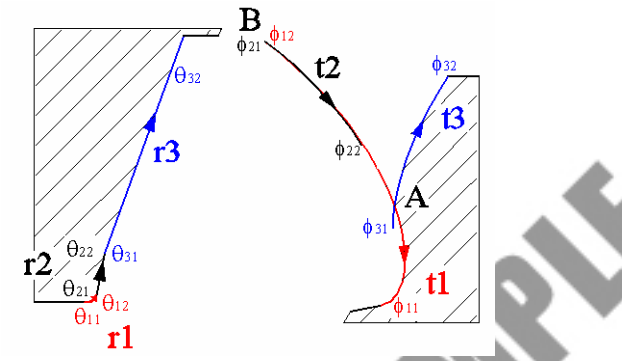

Fig. 3: Extremes values of θ and ϕ.

Using mesh eq. (22) and eq. (27) and written in terms of ϕ yields

$$\phi_e = \frac{x_T + \theta \csc\alpha}{R}$$
$$\phi_t = \frac{x_C - \theta\, \mathrm{ctg}\frac{\theta}{r}}{R} \qquad (30)$$

The first equation refers to the straight line segments r2 and r3 (see fig. 3) of the rack, while the second one refers to the tooth fillet. The limits ϕ can be obtained by substituting into (30) the values for θ found in (19).

Evaluation of intersection points: a numerical technique.

By analysing fig. 3 one can argue that some parts of the envelope curves can be spurious, because of undercutting, i.e. the theoretical curves cannot be practically built.

The actual intersection point A is given by:

$$\begin{cases} x_{t1}(\phi_1) = x_{t3}(\phi_3) \\ y_{t1}(\phi_1) = y_{t3}(\phi_3) \end{cases} \qquad (31)$$

in which x_{t1} and y_{t1} are the expressions (28) and x_{t3} and y_{t3} are the expressions (23) applied to segment r3 of the rack.

Using the Newton technique eq. (31) can be solved iteratively. However, this approach can give rise to numerical troubles. In order to circumvent such problems, eq. (31) can be replaced by considering the distance between two envelope curves; by minimizing such distance one can obtain the intersection point.

The squared distance between two points located on curves t1 and t3 can be expressed as:

$$f(\phi_1, \phi_3) = \left[x_{t1}(\phi_1) - x_{t3}(\phi_3)\right]^2 + \left[y_{t1}(\phi_1) - y_{t3}(\phi_3)\right]^2 \qquad (32)$$

The stationary points of **f** correspond to the zeroes of the gradient:

$$\overline{\nabla} f(\phi_1, \phi_3) = 2 \begin{bmatrix} \frac{d}{d\phi_1} x_{t1}(\phi_1) \cdot \Delta x + \frac{d}{d\phi_1} y_{t1}(\phi_1) \cdot \Delta y \\ -\frac{d}{d\phi_3} x_{t3}(\phi_3) \cdot \Delta x - \frac{d}{d\phi_3} y_{t3}(\phi_3) \cdot \Delta y \end{bmatrix},$$
$$\Delta x = x_{t1}(\phi_1) - x_{t3}(\phi_3)$$
$$\Delta y = y_{t1}(\phi_1) - y_{t3}(\phi_3) \qquad (33)$$

The Newton technique is used to solve eq. (33), i.e. obtain the stationary point; a first trial value for the vector $\overline{\phi}^{(0)}$ is choosen. The stationary points can be minimum, maximum or saddle points. The purpose is to find the minimum; therefore, the following check is considered (k is the number of iterations):

$$f\left(\phi_1^{(k+1)}, \phi_3^{(k+1)}\right) < \varepsilon^2 \qquad (34)$$

For what concern $\overline{\phi}^{(0)}$, geometric considerations yield to choose:

$$\overline{\phi}^{(0)} = \begin{bmatrix} \phi_{32} \\ \phi_{12} \end{bmatrix} \qquad (35)$$

Undercutting

High values of negative addendum modification give rise to undercutting at the tooth base, i.e. close to the intersection between t1 and t2, see fig. 3.

Figure 4 shows how the rack generates spurious envelope branches if it is too close to the wheel.

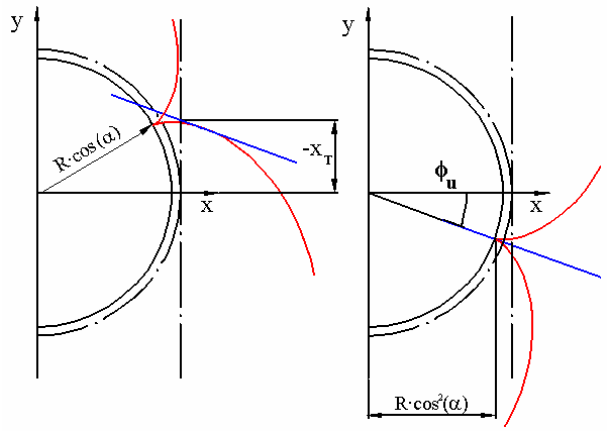

Fig. 4: Generation of spurious enveloped curves by the rack profile

By considering figs. 3 and 4 one finds that a singularity happens for:

$$\phi_{32} < \phi_u \tag{36}$$

The inequality means that the arc profile r3 begins to envelop spurious branch before reaching ϕ_u, at this point the singularity is produced. ϕ_u can be evaluated using eq. (8); moreover, such singular value can be found graphically by observing fig. 4: when the gear angle is ϕ_u the rack has the following translation x_T-R tg(α):

$$\phi_u = \frac{x_T}{R} - tg(\alpha) \tag{37}$$

In the case of undercutting at least two intersections occur: fig. 5 shows the case of undercutting between curves t1 and t3.

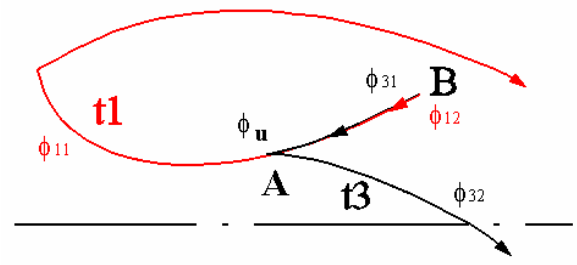

Fig. 5: Intersections between curves t1 and t3

Intersection B is known because it is generated by the limits of the two rack profiles r1 and r3, while the intersection A is evaluated with the previously mentioned numerical method, using ϕ_u instead of ϕ_{12} in eq. (35).

Particular cases

According to the values of the protuberance parameters, two particular cases can be obtained by the enveloping process.

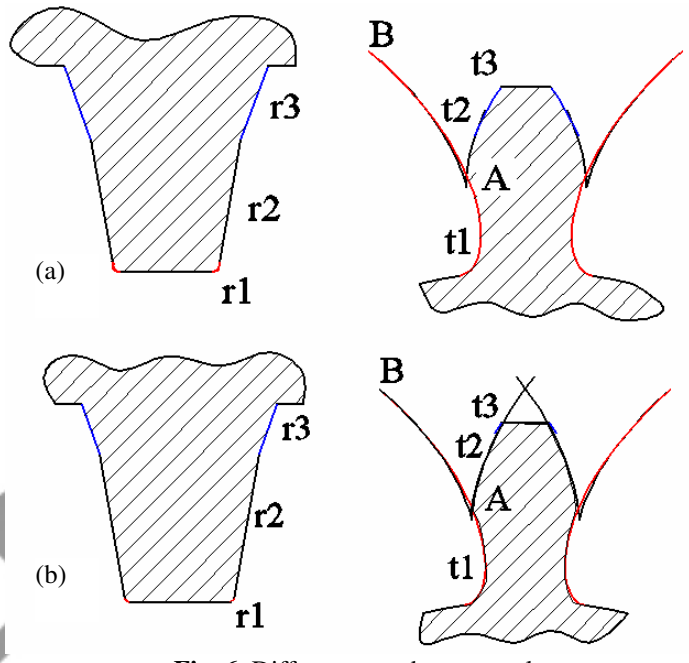

Fig. 6: Different protuberance values

Figure 6 shows two situations, which are theoretical cases and are not included in standard protuberance parameters. In the first case (fig. 6(a)) the protuberance segment r2 generates the small involute curve t2 on the tooth in same way as r3 forms t3. So two intersection A and B must be calculate using numerical method. In the second case the highest values of protuberance r2 annihilates the actual envelope of the segment r3.

A criterion to understand when these two situations occur is to evaluate the intersection ϕ_p between curves t1 and t3. If the segment r2 does not envelop the real tooth flank the following condition must be true:

$$\phi_p > \phi_{31} \tag{38}$$

If the protuberance is such that the segment r3 does not exist, the point correspondent to ϕ_{31} is above the tangent line to the circle tip. This implies:

$$\theta_{31} > \theta_{32} \tag{39}$$

Equations (38) and (39) take into account the curves orientations as in fig. 6.

2D-Gear generator program

All the developed equations were implemented in a FORTRAN code. The code is able to generate an output script file for AutoCAD 2002 containing instructions to draw a complete 2D gear. The input file is insert using dialog box and must contain the following rack and gear information:

- Module;
- Number of teeth;
- Pressure angle;
- Addendum modification;
- Rack fillet radius;
- Protuberance;
- Protuberance angle;

Figure 7 shows different teeth obtained from a rack without protuberance, with pressure angle 20°, module 1 mm and tooth fillet 0.4 mm, using different number of teeth and addendum modification.

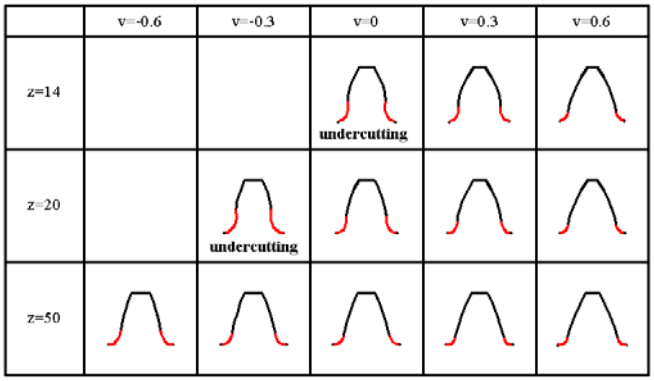

Fig. 7: Example of generated tooth from a rack without protuberance

The code was used to generate the profile of two actual spur gears used in a tractor gearbox, whose parameters are listed below (fig. 8 shows a sample case of generation):

Pinion:

- Module = 3 mm
- Number of teeth = 28
- Pressure angle = 20°
- Addendum modification = 1.927 mm
- Rack fillet radius = 0.1 mm
- Protuberance = 0 mm
- Protuberance angle = 20°

Gear:

- Module = 3 mm
- Number of teeth = 43
- Pressure angle = 20°
- Addendum modification = 2.748 mm
- Rack fillet radius = 0.1 mm
- Protuberance = 0 mm
- Protuberance angle = 20°

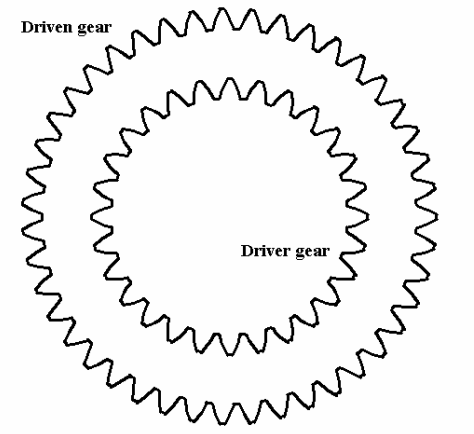

Fig. 8: Driver and driven gear profiles

DYNAMIC MODEL

Using a dynamic approach, spur gear can be modeled with two disks, see fig. 9, coupled by mesh stiffness and mesh damping; the radius of each disk is the base circle radius of the corresponding gear. In this model two assumptions are introduced: no tooth separation between contact teeth and no manufacturing errors on the gears.

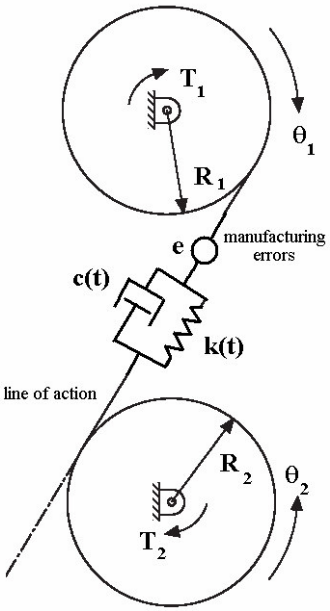

Fig. 9: Dynamic model

The rotational equations of motion of the pinion and gear are

$$I_1\ddot{\vartheta}_1 + c(\dot{x}_1 - \dot{x}_2)R_1 + k(x_1 - x_2)R_1 = T_1 \quad (40)$$

$$I_2\ddot{\vartheta}_2 - c(\dot{x}_1 - \dot{x}_2)R_2 - k(x_1 - x_2)R_2 = -T_2 \quad (41)$$

Where x_1 and x_2 are displacements along the line of action due to rotations ϑ_1 and ϑ_2 respectively.

Considering that $x_i = \vartheta_i R_i$, i=1,2 one can combine eq. (40) and eq. (41); the resulting differential equation for the transmission error is:

$$(\ddot{x}_1 - \ddot{x}_2)\frac{I_1 I_2}{R_1^2 I_2 + R_2^2 I_1} + c(\dot{x}_1 - \dot{x}_2) + k(x_1 - x_2) = W \quad (42)$$

where $W = \frac{T_1}{R_1} = \frac{T_2}{R_2}$ is the transmitted load.

Lets us introduce an equivalent-mass of the dynamical system (42):

$$m = \frac{I_1 I_2}{R_1^2 I_2 + R_2^2 I_1} \quad (43)$$

and the transmission error z along the line of action:

$$z = x_1 - x_2 \quad (44)$$

The resulting equation is:

$$m\ddot{z}(t) + c(t)\dot{z}(t) + k(t)z(t) = W \quad (45)$$

In this case z represents the transmission error due to deformation between the gears during meshing. In eq. (45) both damping and stiffness coefficients are time variable. In the following the damping effect is neglected; indeed, the evaluation of c(t) is beyond the purpose of the present work.

Stiffness evaluation

A 2D finite elements analysis is applied to calculate stiffness. MSC-MARC 2003 is used to perform the analysis. In the analysis the whole gears are considered, neglecting teeth which are not involved in the meshing. In the present case only three teeth per gear are modeled, without loss of accuracy. More than 2400 quadrilateral elements (MARC Quad mesh) are used for each gear (fig. 10). The mesh of the teeth is more refined than the mesh of the wheels bodies, because the deformation is almost completely localized to the teeth.

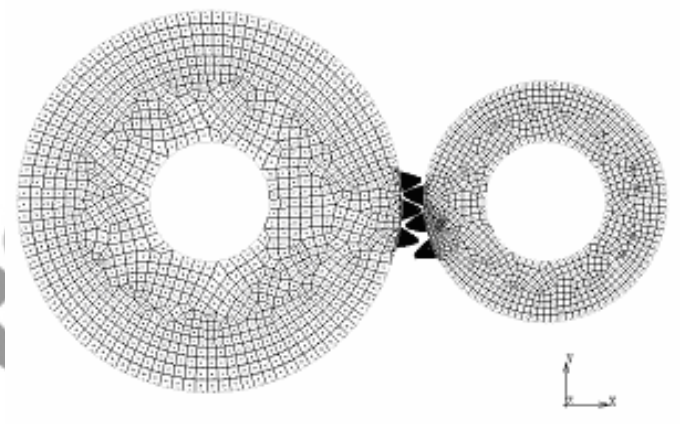

Fig. 10: Mesh of the fem model

The driven wheel shaft is considered locked, i.e. the inner circumference of this wheel has zero rotation. This means that the driven wheel can be deformed around its shaft. The shaft elasticity is not considered here. The driver wheel can rotate around its shaft, i.e. its internal circumference has only rigid rotation.

A torque of C=470.71878 Nm is applied to the driver wheel through its shaft The wheel material is an alloy steel with a Young modulus of $E=2.06*10^{11}$ N/m^2 and Poisson ratio $\nu=0.3$.

Using a center distance of 111 mm the contact ratio becomes $\varepsilon_\alpha=1.6$ [16] with period mesh angle $\overline{\vartheta}$ equal to 12.857°. Fifteen positions are analyzed in order to obtain the driver shaft rotation δ. According to the contact ratio $\varepsilon_\alpha=1.6$, for the first seven positions two pairs of teeth are in contact, while for the remaining positions one pair of teeth is in contact. In the contact regions, see fig. 11, "contact elements" have been used.

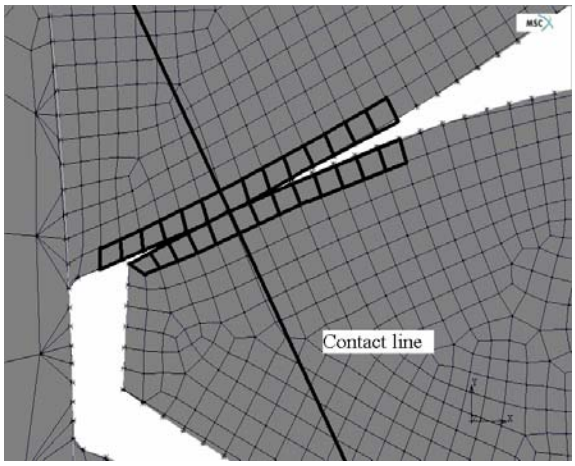

Fig. 11: Contact elements along contact line

The stiffness k is evaluated for each position by using the following relationship which also transforms the torsion stiffness, C/δ_i , into the linear stiffness by dividing it by the square of the base circle radius of the pinion:

$$k_i = \frac{C}{R_1^2 \delta_i} \quad \text{i=1,..,15} \tag{46}$$

The stiffness k depends on the angular position ϑ of the driver wheel, its period is $\overline{\vartheta}$. This periodic function is expanded as Fourier series; the angle ϑ is normalized in order to have a period angle equal to 2π:

$$\tilde{\vartheta} = \frac{\vartheta}{\overline{\vartheta}} 2\pi \tag{47}$$

The Fourier expansion has the following general form:

$$k\left(\tilde{\vartheta}\right) = \tilde{d}_0 + \sum_{i=1}^{N} \tilde{d}_i \cos\left(i\tilde{\vartheta} + \varphi_i\right) \tag{48}$$

where $\tilde{d}_i$ and φ_i are Fourier expansion coefficients.

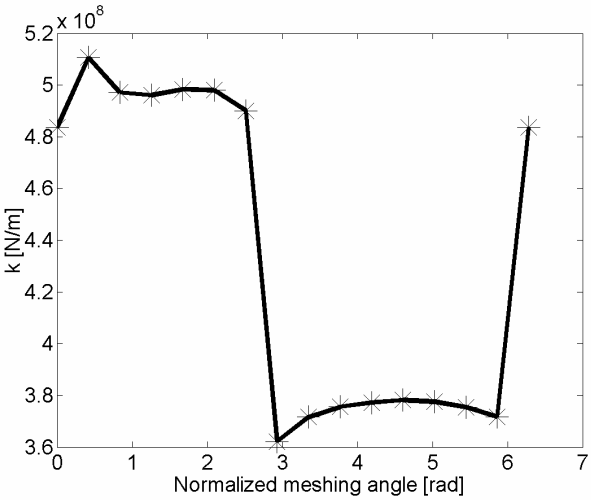

Fig.12: Comparison between analytical function of k (-) and numerical values of k (*)

The computed stiffness and its series expansion is shown in fig. 12, where N=7 is considered.

Neglecting damping and the transmitted load and introducing eq. (48) into eq. (45) yields

$$\ddot{z} + \left(d_0 + \sum_{i=1}^{+\infty} d_i \cos\left(i\omega_f t + \varphi_i\right) \right) z = 0 \tag{49}$$

where $d_i = \tilde{d}_i / m$.

Perturbation solution

Equation (49) is a second order differential equation with time depending coefficients, no exact closed form solutions are available. In this paper the method of multiple scales is used to obtain an approximate solution, which furnishes instability regions of the system.

The solution is expanded in power series of a small parameter ε; moreover, multiple time scales are introduced in order to consider fast and slow time variations [14].

Following the procedure described by Nayfeh and Mook [14] let us introduce a set of new independent variables T_i (fast and slow scales):

$$T_0 = t$$
$$T_1 = \varepsilon t \qquad (50)$$
$$T_2 = \varepsilon^2 t$$

The derivatives with respect to *t* become:

$$\frac{d}{dt} = D_0 + \varepsilon D_1 + \varepsilon^2 D_2$$
$$\frac{d^2}{dt^2} = D_0^2 + 2\varepsilon D_0 D_1 + \varepsilon^2 \left(D_1^2 + 2D_0 D_2\right) \qquad (51)$$

where D_i are partial derivatives respect to T_i.

Let us expand the solution *z* as a power series in ε:

$$z(t,\varepsilon) = z_0(T_0, T_1, T_2) + \varepsilon z_1(T_0, T_1, T_2) + \varepsilon^2 z_2(T_0, T_1, T_2) + \varepsilon^3 z_3(T_0, T_1, T_2) + O(\varepsilon^3) \qquad (52)$$

Substituting eq. (51) and (52) into eq. (49), neglecting φ_i with i=1,..,4, yields to:

$$D_0^2 z_0 + d_0 z_0 = 0 \qquad (53)$$

$$D_0^2 z_1 + d_0 z_1 = -2D_0 D_1 z_0 - P z_0 \qquad (54)$$

$$D_0^2 z_2 + d_0 z_2 = -2D_0 D_1 z_1 - P z_1 - (D_1^2 + 2D_0 D_2) z_0 \qquad (55)$$

$$D_0^2 z_3 + d_0 z_3 = -2D_0 D_1 z_2 - P z_2 - \left(D_1^2 + 2D_0 D_2\right) z_1 - \left(2D_0 D_3 + 2D_1 D_2\right) z_0 \qquad (56)$$

where *P* is:

$$P = \cos(\omega_f t) + \alpha \cos(2\omega_f t) + \beta \cos(3\omega_f t) + \gamma \cos(4\omega_f t) \qquad (57)$$

with:

$$\varepsilon = d_1; \alpha = \frac{d_2}{d_1}; \beta = \frac{d_3}{d_1}; \gamma = \frac{d_4}{d_1} \qquad (58)$$

Equations (53), (54), (55) and (56) are obtained equating the coefficients of ε^0, ε^1, ε^2 and ε^3 to zero.

The solution of eq. (53) is:

$$z_0(T_0, T_1, T_2) = A(T_1, T_2) e^{j\omega T_0} + \overline{A}(T_1, T_2) e^{-j\omega T_0} \qquad (59)$$

where: $d_0=\omega^2$, $\overline{A}$ is the complex conjugate of A.

Inserting eq. (59) into (54) we have:

$$D_0^2 z_1 + d_0 z_1 = -2j\omega D_1 A e^{j\omega T_0}$$
$$-\frac{1}{2}(A e^{j(\omega_f+\omega)T_0} + \alpha A e^{j(2\omega_f+\omega)T_0} + \beta A e^{j(3\omega_f+\omega)T_0} + \gamma A e^{j(4\omega_f+\omega)T_0}$$
$$+\overline{A} e^{j(\omega_f-\omega)T_0} + \alpha \overline{A} e^{j(2\omega_f-\omega)T_0} + \beta \overline{A} e^{j(3\omega_f-\omega)T_0} + \gamma \overline{A} e^{j(4\omega_f-\omega)T_0}) + C.C. \qquad (60)$$

where *C.C.* means complex conjugates terms. At ε^1 level every harmonic generates two forcing terms whose frequencies are ($n\omega_f$–ω) and ($n\omega_f$ +ω). The previous consideration allows to consider each harmonic contribution separately.

Secular terms

In eq. (60) the following secular term is identified:

$$-2j\omega D_1 A e^{j\omega T_0} \qquad (61)$$

Such a term gives rise to spurious divergent solutions and must be removed. Depending on the value of ω four cases are possible:

1. $\omega_f - \omega = \omega \rightarrow \omega_f = 2\omega;$
2. $2\omega_f - \omega = \omega \rightarrow \omega_f = \omega;$
3. $3\omega_f - \omega = \omega \rightarrow \omega_f = \frac{2}{3}\omega;$
4. $4\omega_f - \omega = \omega \rightarrow \omega_f = \frac{\omega}{2};$

Case 1: $\omega_f = 2\omega$

Eliminating secular terms gives

$$-2j\omega D_1 A e^{j\omega T_0} - \frac{1}{2}\overline{A}e^{j(\omega_f-\omega)T_0} = 0 \quad (62)$$

Assuming $\omega_f = \omega+\varepsilon\sigma$, where σ is a detuning parameter, and $D_1A=A'$ and considering that $T_1=\varepsilon T_0$, eq. (62) becomes:

$$-2j\omega A' - \frac{1}{2}\overline{A}e^{j\sigma T_1} = 0 \quad (63)$$

Since A is a complex number depending on T_1, it can be express as follow:

$$A(T_1) = B(T_1)e^{j\frac{\sigma}{2}T_1} \quad (64)$$

where $B(T_1)$ is complex function, eq. (63) becomes:

$$-2j\omega B' + \omega\sigma B - \frac{\overline{B}}{2} = 0 \quad (65)$$

Equation (65) can be decomposed into its real and imaginary parts:

$$\begin{cases} 2\omega B_I' + \omega\sigma B_R - \frac{B_R}{2} = 0 \\ -2\omega B_R' + \omega\sigma B_I + \frac{B_I}{2} = 0 \end{cases} \quad (66)$$

where $B=B_I+jB_R$.

Assuming that $B(T_1) = (G_R + jG_I)e^{\xi T_1}$ we can write eq. (66) in a matrix form:

$$\xi\begin{bmatrix} 0 & 2\omega \\ -2\omega & 0 \end{bmatrix}\begin{bmatrix} G_R \\ G_I \end{bmatrix} + \begin{bmatrix} \omega\sigma - \frac{1}{2} & 0 \\ 0 & \omega\sigma + \frac{1}{2} \end{bmatrix}\begin{bmatrix} G_R \\ G_I \end{bmatrix} = \begin{bmatrix} 0 \\ 0 \end{bmatrix} \quad (67)$$

System (66) and (67) are equivalent and the solution can be found imposing:

$$\left(\xi\begin{bmatrix} 0 & 2\omega \\ -2\omega & 0 \end{bmatrix} + \begin{bmatrix} \omega\sigma - \frac{1}{2} & 0 \\ 0 & \omega\sigma + \frac{1}{2} \end{bmatrix}\right)\begin{bmatrix} G_R \\ G_I \end{bmatrix} = \begin{bmatrix} 0 \\ 0 \end{bmatrix} \quad (68)$$

This eq. has non trivial solution if the determinant of its matrix is equal to zero, which means:

$$\xi^2 = \frac{1}{4\omega^2}\left(\frac{1}{4} - \omega^2\sigma^2\right) \quad (69)$$

Instability occurs when $\xi^2>0$, i.e. when:

$$\left(\frac{1}{4} - \omega^2\sigma^2\right) > 0 \quad (70)$$

Remembering that $\varepsilon=d_1$ and substituting $\sigma = \frac{\omega_f - 2\omega}{\varepsilon}$ into (70) yields:

$$2\sqrt{d_0} - \frac{d_1}{2\sqrt{d_0}} < \omega_f < 2\sqrt{d_0} + \frac{d_1}{2\sqrt{d_0}} \quad (71)$$

The same approach is applied to cases 2, 3, and 4.

Case 2: $\omega_f = \omega$

In this case the detuning parameter σ is:

$$\sigma = \frac{2\omega_f - 2\omega}{\varepsilon} \tag{72}$$

which leads to the following instability region:

$$\sqrt{d_0} - \frac{d_2}{4\sqrt{d_0}} < \omega_f < \sqrt{d_0} + \frac{d_2}{4\sqrt{d_0}} \tag{73}$$

Case 3: $\omega_f = \frac{2}{3}\omega$

In this case the detuning parameter σ is:

$$\sigma = \frac{3\omega_f - 2\omega}{\varepsilon} \tag{74}$$

which leads to the following instability region:

$$\frac{2}{3}\sqrt{d_0} - \frac{d_3}{6\sqrt{d_0}} < \omega_f < \frac{2}{3}\sqrt{d_0} + \frac{d_3}{6\sqrt{d_0}} \tag{75}$$

Case 4: $\omega_f = \frac{\omega}{2}$

In this case the detuning parameter σ is:

$$\sigma = \frac{4\omega_f - 2\omega}{\varepsilon} \tag{76}$$

which leads to the following instability region:

$$\frac{\sqrt{d_0}}{2} - \frac{d_4}{8\sqrt{d_0}} < \omega_f < \frac{\sqrt{d_0}}{2} + \frac{d_4}{8\sqrt{d_0}} \tag{77}$$

In Tab.1 the instability regions for the gear pair under investigation is presented:

Case	Instability region [rad/s]
1	$62993 < \omega_f < 68945$
2	$32728 < \omega_f < 33241$
3	$21642 < \omega_f < 22338$
4	$16364 < \omega_f < 16621$

Tab. 1:Instabilty regions expressed on meshing frequency $\omega_{f.}$

Considering that:

$$\Omega_p = \frac{60\omega_f}{2\pi z_1} \tag{78}$$

The instability regions are reported in Tab. 2 in terms of the driver gear velocity Ω_p.

Case	Instability region [rpm]	$\Delta\Omega_p$ [rpm]
1	$21484 < \Omega_p < 23514$	2030
2	$11162 < \Omega_p < 11337$	175
3	$7381 < \Omega_p < 7618$	237
4	$5581 < \Omega_p < 5669$	88

Tab. 2: Instability regions expressed on driver gear velocity $\Omega_{p.}$

CONCLUSION

In this paper instability regions for a single degrees of freedom gear model have been evaluated using multiple time scales perturbation technique. Damping, tooth separation between contact teeth and manufacturing errors

are neglected. Analytical steps allow to consider each harmonic contribution separately, by means of which four different cases are analyzed separately using different detuning parameters σ.

One case study is analyzed. Four instability regions for the driver gear velocity have been obtained, modeling teeth profiles and mesh stiffness with the approach described above. Results show instability regions occur at about 22500, 11250, 7500 and 5600 rpm. Such high values can be justified by the assumption of neglecting shafts and bears effects on the meshing stiffness. Future development in fem model are required in order to consider the previous mentioned effects. Instability regions formulas are still applicable and can be effectively used with different values of stiffness Fourier expansion coefficients.

ACKNOWLEDGMENTS

Acknowledgments to CNH Italy for supplied support.

REFERENCES

[1] Ozguven, H.N., Houser, D.R., 1988, "Dynamic analysis of high speed gears by using loaded static transmission error", Journal of Sound and Vibration, **125**, pp.83.

[2] Andersson, A., Vedmar, L., 2003, "A dynamic model to determine vibrations in involute helical gears", Journal of Sound and Vibration, **260**, pp. 195-212.

[3] Yang, D.C.H., Sun, Z.S., December 1985, "A rotary model for spur gear dynamics", Journal of Mechanisms, Transmission, and Automation in Design, **107**, pp. 530-535.

[4] Lin, H.-H., Huston, R.L., Coy, J.J., June 1988, "On dynamic loads in parallel shaft transmissions: Part I – Modelling and analysis", Journal of Mechanisms, Transmission, and Automation in Design, **110**, pp. 221-225.

[5] Lin, H.-H., Huston, R.L., Coy, J.J., June 1988, "On dynamic loads in parallel shaft transmissions: Part II – Parameter study", Journal of Mechanisms, Transmission, and Automation in Design, **110**, pp. 226-229.

[6] Cai, Y., Hayashi, T., June 1994, "The linear approximated equation of vibration of a pair of spur gears (Theory and experiment)", Journal of Mechanical Design, **116**, pp. 558-564.

[7] Parker, R.G., Vijayakar, S.M., Imajo, T. , 2000, "Non-linear dynamic response of a spur gear pair: modelling and experimental comparisons", Journal of Sound and Vibration, **237(3)**, pp. 435-455.

[8] Amabili, M., Rivola, 1997, "Dynamic analysis of spur gear pairs: steady-state response and stability of the sdof model with time-varying meshing damping", Mechanical Systems and Signal Processing, **11(3)**, 375-390.

[9] Tsai, M.-H., Tsai, Y.-C., 1997, "A method for calculating static transmission errors of plastic spur gears using FEM evaluation", Finite Elements in Analysis and Design, **27**, 345-357.

[10] M.S. Tavakoli, D.R. Houser, 1986, "Optimum profile modifications for the minimization of static transmission errors of spur gears", Journal of Mechanical Design, **108**, 86-95.

[11] Howard, I., Jia, S., Wang, J., 2001, "The dynamic modelling of a spur gear in mesh including friction and a crack", Mechanical Systems and Signal Processing, **15(5)**, 831-853.

[12] Zalgaller, V.A., Litvin, F.L., "Sufficient condition of existence of envelope to contact lines and edge of regression on the surface for the envelope to the family of surfaces represented in parametric form", Proceedings of Universities: Mathematics 3, **178**, 20-23 (in Russian).

[13] Litvin, F.L., Demenego, A., Vecchiato, D., 2001, "Formation by branches of envelope to parametric families of surfaces and curves", Computer Methods in Applied Mechanics and Engineering, **190**, 4587-4608.

[14] Nayfeh, A., H., Mook, D.,T., 1979, Nonlinear oscillations, John Wiley & Sons, New York.

[15] UNI 8862/2, 1998 "Cylindrical gears for general and heavy engineering -- Standard basic rack tooth profile".

[16] ISO 1122-1, 1998 "Vocabulary of gear terms -- Part 1: Definitions related to geometry".